Some Aspects of the Method of Fundamental Solutions for Certain Biharmonic Problems

Yiorgos-Sokratis Smyrlis & Andreas Karageorghis

Department of Mathematics and Statistics
University of Cyprus/ $\Pi\alpha\nu\epsilon\pi\iota\sigma\tau\acute{\eta}\mu\iota o$ $K\acute{\upsilon}\pi\rho o\upsilon$, P.O. Box 20537
1678 Nicosia/$\Lambda\epsilon\upsilon\kappa\omega\sigma\acute{\iota}\alpha$, Cyprus/$K\acute{\upsilon}\pi\varrho o\varsigma$

Abstract

In this study, we investigate the application of the Method of Fundamental Solutions for the solution of biharmonic Dirichlet problems on a disk. Modifications of the method for overcoming sources of inaccuracy are suggested. We also propose an efficient algorithm for the solution of the resulting systems which exploits the symmetries of the matrices involved. The techniques described in the paper are applied to standard test problems.

1 Statement of the problem

The Method of Fundamental Solutions (MFS) is a *meshless* method applicable to certain elliptic boundary value problems. Recently, because of the advantages that meshless methods possess over other boundary methods and domain discretization methods, there has been an increase in the interest in the MFS. The MFS was first proposed by Alexidze and Kupradze [11, 12] and in its modern numerical version by Mathon and Johnston [15]. Recent surveys of MFS-type methods are given in [5] and [7]. Also, a wide range of applications of the MFS can be found in [10], whereas the application of MFS-type methods to acoustic and electromagnetic scattering problems is described in [4].

The application of the MFS to the Dirichlet problem for Laplace's equation in a disk as well as various theoretical aspects of the method was the subject of a recent study [18]. The MFS was applied to biharmonic problems in [2] and [8], respectively. Details of various MFS biharmonic formulations may be found in [5] and references therein.

In this paper, we consider the boundary value problem

$$\begin{cases} \Delta^2 u = 0 & \text{in} \quad \Omega, \\ u = f & \text{on} \quad \partial\Omega\,, \\ \dfrac{\partial u}{\partial n} = g & \text{on} \quad \partial\Omega\,, \end{cases} \tag{1.1}$$

where Δ denotes the Laplace operator and f and g are given functions, and Ω is the disk of radius ϱ,

$$\Omega = \{\boldsymbol{x} \in \mathbb{R}^2 \, : \, |\boldsymbol{x}| < \varrho\} \,. \tag{1.2}$$

Motivated by the simple layer potential representation of [14], in the biharmonic MFS with fixed singularities [5, 11, 15], the solution u is approximated by

$$u_N(P; \boldsymbol{\mu}, \boldsymbol{\nu}, \boldsymbol{Q}) \; = \; \sum_{j=1}^{N} \left[\mu_j \, k_1(P, Q_j) + \nu_j \, k_2(P, Q_j)\right], \qquad P \in \overline{\Omega}, \tag{1.3}$$

where $\boldsymbol{\mu} = (\mu_1, \mu_2, \ldots, \mu_N)^T$, $\boldsymbol{\nu} = (\nu_1, \nu_2, \ldots, \nu_N)^T$ and $\boldsymbol{Q}$ is a $2N$-vector containing the coordinates of the singularities Q_j, $j = 1, \ldots, N$, which lie outside $\overline{\Omega}$. The function $k_1(P, Q)$ is a fundamental solution of Laplace's equation given by

$$k_1(P, Q) = -\frac{1}{2\pi} \log |P - Q|, \tag{1.4}$$

and the function $k_2(P, Q)$ is a fundamental solution of the biharmonic equation given by

$$k_2(P, Q) = -\frac{1}{8\pi} |P - Q|^2 \log |P - Q|, \tag{1.5}$$

with $|P - Q|$ denoting the distance between the points P and Q. The singularities Q_j are fixed on the boundary $\partial\tilde{\Omega}$ of a disk $\tilde{\Omega}$ concentric to Ω and defined by $\tilde{\Omega} = \{\boldsymbol{x} \in \mathbb{R}^2 : |\boldsymbol{x}| < R\}$, where $R > \varrho$. A set of equally spaced collocation points $\{P_i\}_{i=1}^N$ is chosen on $\partial\Omega$, so that if $P_i = (x_{P_i}, y_{P_i})$, then

$$x_{P_i} = \varrho \cos \frac{2(i-1)\pi}{N}, \;\; y_{P_i} = \varrho \sin \frac{2(i-1)\pi}{N}, \;\; i = 1, \ldots, N \,. \tag{1.6}$$

If $Q_j = (x_{Q_j}, y_{Q_j})$, then

$$x_{Q_j} = R \cos \frac{2(j-1)\pi}{N}, \;\; y_{Q_j} = R \sin \frac{2(j-1)\pi}{N}, \;\; j = 1, \ldots, N \,. \tag{1.7}$$

The vectors of coefficients $\boldsymbol{\mu}$ and $\boldsymbol{\nu}$ are determined so that the boundary conditions are satisfied at the collocation points $\{P_i\}_{i=1}^N$:

$$u_N(P_i; \boldsymbol{\mu}, \boldsymbol{\nu}, \boldsymbol{Q}) = f(P_i), \;\; i = 1, \ldots, N, \tag{1.8}$$

and

$$\frac{\partial u_N}{\partial n}(P_i; \boldsymbol{\mu}, \boldsymbol{\nu}, \boldsymbol{Q}) = g(P_i), \;\; i = 1, \ldots, N. \tag{1.9}$$

This yields a $2N \times 2N$ linear system of the form

$$G^0 \left(\frac{\boldsymbol{\mu}}{\boldsymbol{\nu}}\right) \; = \; \left(\frac{\boldsymbol{f}}{\boldsymbol{g}}\right), \tag{1.10}$$

where

$$G^0 \; = \; \left(\begin{array}{c|c} A^0 & B^0 \\ \hline C^0 & D^0 \end{array}\right)$$

with the $N \times N$ matrices $A^0 = \left(A^0_{i,j}\right)$, $B^0 = \left(B^0_{i,j}\right)$, $C^0 = \left(C^0_{i,j}\right)$ and $D^0 = \left(D^0_{i,j}\right)$, where

$$A^0_{i,j} = -\frac{1}{2\pi} \log |P_i - Q_j|, \tag{1.11}$$

$$B^0_{i,j} = -\frac{1}{8\pi} |P_i - Q_j|^2 \log |P_i - Q_j|, \tag{1.12}$$

$$C^0_{i,j} = -\frac{1}{2\pi} \left(\frac{x_{P_i} - x_{Q_j}}{|P_i - Q_j|^2} n_x + \frac{y_{P_i} - y_{Q_j}}{|P_i - Q_j|^2} n_y \right), \tag{1.13}$$

$$D^0_{i,j} = -\frac{1}{8\pi} \left[1 + 2 \log |P_i - Q_j|\right] \left((x_{P_i} - x_{Q_j}) n_x + (y_{P_i} - y_{Q_j}) n_y \right), \quad i, j = 1, \ldots, N, \tag{1.14}$$

and n_x and n_y denote the components of the outward normal vector $\boldsymbol{n}$ to $\partial\Omega$ in the x and y directions, respectively. The matrices A^0, B^0, C^0 and D^0 are *circulant**

In earlier work [18], as well as in the current study, we observed, that the accuracy of the MFS solution is poor when the singularities are placed very close to $\partial\Omega$. This problem, in the present case, arises because our approach may be viewed as attempting to approximate an integral of the form (see [14])

$$I(P) = \int_{\partial\Omega} \nu(Q) |P - Q|^2 (\log |P - Q| - 1)\, ds(Q) + \int_{\partial\Omega} \mu(Q) \log |P - Q| ds(Q)$$

by a quadrature rule. As we approach the boundary, the integrand becomes singular and the quadrature rule becomes progressively less accurate.

Also, the accuracy of the MFS is poor when the singularities are placed very far from the boundary, i.e. on a circle of radius $R \gg \varrho$. This problem arises because as we move away from the boundary the matrix G^0 becomes ill-conditioned. This can lead to large errors in the MFS approximation (see [6]). The behaviour of the conditioning of the matrix G^0 for various numbers of degrees of freedom $N = 2^n$, $n = 3, 4, \ldots, 10$; as $\varepsilon = R - \varrho$ varies, can be seen from figure 1. In this figure, we plot the logarithm of the condition number versus the logarithm of ε. The condition number κ_∞ of G_0 in the L_∞ norm, is calculated with the NAG pair F07ADF-F07AGF [17]. From the figure, we observe that for sufficiently small ε, namely $\varepsilon < 10^{-1}$ for $N = 8$ to $\varepsilon < 10^{-2}$ for $N = 1024$, and intermediate values for the other values of N presented, the condition number decreases algebraically with ε, while increasing with N. On the contrary, for larger values of ε, the condition number grows exponentially.

In this work, we address the above two problems, namely

---

*A square matrix A is circulant (see [3]) if it has the form

$$A = \begin{pmatrix} a_1 & a_2 & \cdots & a_N \\ a_N & a_1 & \cdots & a_{N-1} \\ \vdots & \vdots & & \vdots \\ a_2 & a_3 & \cdots & a_1 \end{pmatrix}. \tag{1.15}$$

This means that the elements of each row are same as the elements of the previous row but moved one position to the right. The first element of each row is the same as the the last element of the previous row. The circulant matrix A in (1.15) is usually denoted by $A = circ(\mathbf{a})$, where $\mathbf{a} = circ(a_1, a_2, \ldots, a_N)$. Properties of circulant matrices are given in Section 3.1.

- the loss of accuracy when the singularities are placed very close to the boundary, i.e. $\varepsilon \ll 1$ *and*
- the loss of accuracy when the singularities are placed very far to the boundary, i.e. $\varepsilon \gg 1$.

2 Rotation and normalization

2.1 Rotation of the singularities

As in [18], we study the behaviour of the error as the positions of the singularities are *rotated*. If we denote the coordinates of the singularity Q_j^α by $x_{Q_j^\alpha}$ and $y_{Q_j^\alpha}$, these become

$$x_{Q_j^\alpha} = R\cos\frac{2(j-1+\alpha)\pi}{N}, \quad y_{Q_j^\alpha} = R\sin\frac{2(j-1+\alpha)\pi}{N}, \quad j=1,\ldots,N, \tag{2.1}$$

where $0 \leq \alpha < 1$. This means that the positions of the singularities differ by an angle $2\pi\alpha/N$ from the positions of the boundary points. The satisfaction of the boundary conditions

$$u_N(P_i;\boldsymbol{\mu},\boldsymbol{\nu},\boldsymbol{Q}^\alpha) = f(P_i), \quad \frac{\partial u_N}{\partial n}(P_i;\boldsymbol{\mu},\boldsymbol{\nu},\boldsymbol{Q}^\alpha) = g(P_i), \quad i=1,\ldots,N\,,$$

now yields a linear system of the form

$$G^\alpha \left(\frac{\boldsymbol{\mu}}{\boldsymbol{\nu}}\right) = \left(\frac{\boldsymbol{f}}{\boldsymbol{g}}\right), \tag{2.2}$$

where

$$G^\alpha = \left(\begin{array}{c|c} A^\alpha & B^\alpha \\ \hline C^\alpha & D^\alpha \end{array}\right) \tag{2.3}$$

and

$$A_{i,j}^\alpha = -\frac{1}{2\pi}\log|P_i - Q_j^\alpha|, \tag{2.4}$$

$$B_{i,j}^\alpha = -\frac{1}{8\pi}|P_i - Q_j^\alpha|^2\log|P_i - Q_j^\alpha|, \tag{2.5}$$

$$C_{i,j}^\alpha = -\frac{1}{2\pi}\left(\frac{x_{P_i} - x_{Q_j^\alpha}}{|P_i - Q_j^\alpha|^2}n_x + \frac{y_{P_i} - y_{Q_j^\alpha}}{|P_i - Q_j^\alpha|^2}n_y\right), \tag{2.6}$$

$$D_{i,j}^\alpha = -\frac{1}{8\pi}\left[1 + 2\log|P_i - Q_j^\alpha|\right]\left((x_{P_i} - x_{Q_j^\alpha})n_x + (y_{P_i} - y_{Q_j^\alpha})n_y\right), \quad i,j=1,\ldots,N\,. \tag{2.7}$$

As in the case $\alpha = 0$, the matrices A^α, B^α, C^α and D^α are circulant. In the present work, we only studied the effect of rotating the singularities by an angular parameter α, where $\alpha \in [0, 1/2)$, because of the symmetry of the geometry about $\alpha = 1/2$. Also, at $\alpha = 1/2$ the matrix G^α is singular:

Lemma When $N = 2m$, $m \in \mathbb{N}$, the matrix $G^{\frac{1}{2}}$ is singular.

Proof. In this case the matrices $A^{\frac{1}{2}}, B^{\frac{1}{2}}, C^{\frac{1}{2}}$ and $D^{\frac{1}{2}}$ are of the form $circ(a_1, a_2, \ldots, a_m, a_m, a_{m-1}, \ldots, a_1)$, $circ(b_1, b_2, \ldots, b_m, b_m, b_{m-1}, \ldots, b_1)$, $circ(c_1, c_2, \ldots, c_m, c_m, c_{m-1}, \ldots, c_1)$, and $circ(d_1, d_2, \ldots, d_m, d_m, d_{m-1}, \ldots, d_1)$, respectively. It is sufficient to observe that the sum of the first m odd rows of the matrix $G^{\frac{1}{2}}$ is equal to the sum of the first m even rows of $G^{\frac{1}{2}}$.

□

As will become apparent in the numerical results section, the rotation of the singularities can improve the accuracy of the MFS approximation.

2.2 Normalization

When R is large, the poor conditioning of the matrices G^α (see Figure 1) and the loss of significance, can lead to poor results. The loss of significance is a result of the presence of elements of very large size which are almost identical for large R, in each of the four circulant matrices A^α, B^α, C^α and D^α. For example, in A^α all the elements satisfy the inequalities

$$-\frac{1}{2\pi}\log(R+\varrho) \;\le\; A^\alpha_{i,j} \;\le\; -\frac{1}{2\pi}\log(R-\varrho)\,.$$

As in [18], in order to improve the accuracy of the MFS we consider a form of scaling by using the *normalized* fundamental solutions

$$\tilde{k}_1(P,Q) = -\frac{1}{2\pi}\log\frac{|P-Q|}{R}, \tag{2.8}$$

and

$$\tilde{k}_2(P,Q) = -\frac{1}{8\pi}\frac{|P-Q|^2}{R^2}\log\frac{|P-Q|}{R}\,, \tag{2.9}$$

then

$$\tilde{G}^\alpha = \left(\begin{array}{c|c} \tilde{A}^\alpha & \tilde{B}^\alpha \\ \hline \tilde{C}^\alpha & \tilde{D}^\alpha \end{array}\right)$$

where

$$\tilde{A}^\alpha_{i,j} = -\frac{1}{2\pi}\log\frac{|P_i-Q^\alpha_j|}{R}, \tag{2.10}$$

$$\tilde{B}^\alpha_{i,j} = -\frac{1}{8\pi}\frac{|P_i-Q^\alpha_j|^2}{R^2}\log\frac{|P_i-Q^\alpha_j|}{R}, \tag{2.11}$$

$$\tilde{C}^\alpha_{i,j} = -\frac{1}{2\pi}\left(\frac{x_{P_i}-x_{Q^\alpha_j}}{|P_i-Q^\alpha_j|^2}n_x + \frac{y_{P_i}-y_{Q^\alpha_j}}{|P_i-Q^\alpha_j|^2}n_y\right), \tag{2.12}$$

$$\tilde{D}^\alpha_{i,j} = -\frac{1}{8\pi}\left[1+2\log\frac{|P_i-Q^\alpha_j|}{R}\right]\frac{\left((x_{P_i}-x_{Q^\alpha_j})n_x + (y_{P_i}-y_{Q^\alpha_j})n_y\right)}{R^2}, \quad i,j = 1,\ldots,N\,. \tag{2.13}$$

The matrices $\tilde{A}^\alpha, \tilde{B}^\alpha, \tilde{C}^\alpha$ and $\tilde{D}^\alpha$ are circulant.

As will be reported in the numerical results section, the use of normalized fundamental solutions improves the accuracy of the MFS approximation for large values of R.

3 Efficient solution of block circulant system

3.1 Properties of circulant matrices

We shall be using the following properties of circulant matrices: (See Davis [3]).

Properties *Let $A \in \mathbb{C}^{N \times N}$ be a circulant matrix, i.e. $A = circ(a_1, \ldots, a_N)$. Then A is normal, i.e. $AA^* = A^*A$, and thus diagonalizable. In particular, there exists a unitary matrix U and a diagonal matrix $D = \mathrm{diag}(\mu_1, \ldots, \mu_N)$, such that*

$$A = U^* D U ,$$

with eigenvalues

$$\mu_j = \sum_{k=1}^{N} a_k \omega^{(k-1)(j-1)}, \quad j = 1, \ldots, N, \quad \omega = e^{\frac{2\pi i}{N}} ,$$

and corresponding eigenvectors

$$\boldsymbol{\xi}_j = \frac{1}{N^{1/2}} \left(1, \omega^{(j-1)}, \omega^{2(j-1)}, \ldots, \omega^{(n-1)(j-1)}\right) , \quad j = 1, \ldots, N .$$

The vectors $\{\boldsymbol{\xi}_1, \ldots, \boldsymbol{\xi}_N\}$ form an orthonormal basis of $\mathbb{C}^N$. The matrix U is symmetric and its conjugate is the Fourier matrix

$$U^* = \frac{1}{N^{1/2}} \begin{pmatrix} 1 & 1 & 1 & \cdots & 1 \\ 1 & \omega & \omega^2 & \cdots & \omega^{N-1} \\ 1 & \omega^2 & \omega^4 & \cdots & \omega^{2(N-1)} \\ \vdots & \vdots & \vdots & & \vdots \\ 1 & \omega^{N-1} & \omega^{2(N-1)} & \cdots & \omega^{(N-1)(N-1)} \end{pmatrix} .$$

Conversely, for any diagonal matrix D, the matrix $A = U^*DU$ is circulant. Consequently, the product of two circulant matrices is also circulant.

Furthermore, if A is circulant, then A^* is also circulant. If A is circulant and nonsingular, its inverse is also circulant.

Finally, any linear combination of two circulant matrices is also circulant. In particular, if λ, $\mu \in \mathbb{C}$ and $A = circ(\boldsymbol{a})$, $B = circ(\boldsymbol{b})$, then $\lambda A + \mu B = circ(\lambda \boldsymbol{a} + \mu \boldsymbol{b})$.

3.2 Efficient implementation of basic circulant matrix operations

The object of this section is to propose an efficient algorithm for the solution of system (2.2). This is done by exploiting the block circulant structure of G^{α}. Here, the term *block circulant* indicates that that matrix G^{α} can be decomposed into four circulant $N \times N$ matrices (see 2.3). The algorithm relies on the properties of circulant matrices, in particular the fact that basic matrix operations such as multiplication and inversion of can be performed at a cost of $O(N \log N)$ operations ([3, 18].)

3.2.1 Solution of circulant systems

In the solution of the system $A\boldsymbol{x} = \boldsymbol{b}$, where $A = circ(\boldsymbol{a})$, and nonsingular with $A = U^{*}DU$, clearly,

$$\boldsymbol{x} = A^{-1}\boldsymbol{b} = U^{*}D^{-1}U\boldsymbol{b}.$$

The evaluation of $\boldsymbol{x}$ is carried out efficiently in the following four steps:

- **Step 1** Calculation of the vector $\check{\boldsymbol{b}} = U\boldsymbol{b}$ which is simply the *inverse discrete Fourier transform (IDFT)* of the vector $\boldsymbol{b}$. In MATLAB, this operation can be performed using the inverse fast Fourier transform command `ifft(b)`.
- **Step 2** Calculation of the diagonal matrix $D = \mathrm{diag}(\boldsymbol{d})$. The vector $\boldsymbol{d}$ of the diagonal elements of D is simply the *discrete Fourier transform (DFT)* of the vector $\boldsymbol{a}$. In MATLAB, this operation can be performed using the fast Fourier transform command `fft(a)`.
- **Step 3** Evaluation of the vector $\boldsymbol{e} = D^{-1}U\boldsymbol{b}$ which is simply the elements of the vector $U\boldsymbol{b}$ divided by the corresponding elements of the vector of the diagonal elements of D, that is

  $$e_k = \frac{\check{b}_k}{d_k}, \quad k = 1, \ldots, N.$$

  In MATLAB this can be done via `b̌./d`.
- **Step 4** Calculation of vector $\boldsymbol{x} = U^{*}\boldsymbol{e}$ which is simply the *DFT* of $\boldsymbol{e}$. In MATLAB this is carried out by `fft(e)`.

Summarizing, we observe that steps 1,2,4 require three Fourier transforms, hence $O(N \log N)$ operations. Step 3 requires only $O(N)$ operations. In MATLAB the calculation of $\boldsymbol{x}$ can be elegantly summarized as `x=fft(ifft(b)./fft(a))`.

3.2.2 Multiplication and inversion of circulant matrices

In the case when we need to compute the circulant matrix $C = AB$ (resp. $C = A^{-1}B$) where $A = circ(\boldsymbol{a})$ is nonsingular, and $B = circ(\boldsymbol{b})$, steps similar to those described earlier for the solution of the system $A\boldsymbol{x} = \boldsymbol{b}$ can be applied. If $C = circ(\boldsymbol{c})$, then the MATLAB command for the calculation of the vector $\boldsymbol{c}$ is merely `c=ifft(fft(a).*fft(b))` (resp. `c=ifft(fft(b)./fft(a))`). Note that to calculate the inverse of a matrix A, we simply take $B = I$ in the case $C = A^{-1}B$. The cost of any of these matrix operations is $O(N \log N)$ operations.

3.3 Application to block circulant system

Consider the block circulant system

$$G^\alpha \left(\frac{\boldsymbol{\mu}}{\boldsymbol{\nu}} \right) = \left(\begin{array}{c|c} A^\alpha & B^\alpha \\ \hline C^\alpha & D^\alpha \end{array} \right) \left(\frac{\boldsymbol{\mu}}{\boldsymbol{\nu}} \right) = \left(\frac{\boldsymbol{f}}{\boldsymbol{g}} \right), \tag{3.1}$$

which can be written as

$$\left\{ \begin{array}{rcl} A^\alpha \boldsymbol{\mu} + B^\alpha \boldsymbol{\nu} & = & \boldsymbol{f} \\ C^\alpha \boldsymbol{\mu} + D^\alpha \boldsymbol{\nu} & = & \boldsymbol{g}\,. \end{array} \right. \tag{3.2}$$

Provided that A^α is nonsingular, it is easy to see that

$$\left(D^\alpha - C^\alpha [A^\alpha]^{-1} B^\alpha \right) \boldsymbol{\nu} = \boldsymbol{g} - C^\alpha [A^\alpha]^{-1} \boldsymbol{f}, \tag{3.3}$$

where the matrix $S^\alpha = D^\alpha - C^\alpha [A^\alpha]^{-1} B^\alpha$ is the Schur complement of A^α in G^α. Further, S^α is nonsingular if and only if G^α is nonsingular, provided A^α is nonsingular [19]. The system (3.3) can be solved efficiently because the Schur complement matrix S^α is circulant. This follows from the fact that the submatrices $A^\alpha, B^\alpha, C^\alpha$ and D^α are circulant. The construction of the system (3.3) can be performed efficiently as it only involves multiplications and inversions of circulant matrices.

Once $\boldsymbol{\nu}$ has been computed, $\boldsymbol{\mu}$ can be found from

$$\boldsymbol{\mu} = [A^\alpha]^{-1} \left(\boldsymbol{f} - B^\alpha \boldsymbol{\nu} \right). \tag{3.4}$$

More precisely, if

$$A^\alpha = circ(\boldsymbol{a}^\alpha), \;\; B^\alpha = circ(\boldsymbol{b}^\alpha), \;\; C^\alpha = circ(\boldsymbol{c}^\alpha), \;\; D^\alpha = circ(\boldsymbol{d}^\alpha),$$

we have the following **Algorithm**:

- **Step 1** Compute the *DFT* of the vectors $\boldsymbol{a}^\alpha$, $\boldsymbol{b}^\alpha$, $\boldsymbol{c}^\alpha$ and $\boldsymbol{d}^\alpha$, which are denoted by $\boldsymbol{s}^a$, $\boldsymbol{s}^b$, $\boldsymbol{s}^c$ and $\boldsymbol{s}^d$, respectively. These are the diagonals of the diagonal matrices $UA^\alpha U^*$, $UB^\alpha U^*$, $UC^\alpha U^*$ and $UD^\alpha U^*$, respectively. Also, compute the *IDFT* of the vectors $\boldsymbol{f}$ and $\boldsymbol{g}$ which are denoted by $\boldsymbol{s}^f$ and $\boldsymbol{s}^g$.

- **Step 2** Compute the *IDFT* of the vector $\boldsymbol{p} = \boldsymbol{g} - C^\alpha[A^\alpha]^{-1}\boldsymbol{f}$ which is the right hand side of (3.3), and which is denoted by $\boldsymbol{s}^p$. This is obtained with $O(N)$ operations via

  $$s_k^p = s_k^g - s_k^f \cdot s_k^c / s_k^a\,, \quad k = 1, \ldots, N\,.$$

  Also compute the vector $\boldsymbol{s}^q$ which is the diagonal of the diagonal matrix

  $$Q \;=\; U\left(D^\alpha - C^\alpha[A^\alpha]^{-1}B^\alpha\right)U^*\,.$$

  This is also done with $O(N)$ operations via

  $$s_k^q = s_k^d - s_k^f \cdot s_k^b / s_k^a\,, \quad k = 1, \ldots, N\,.$$

  Then we obtain the *IDFT* of the vector $\boldsymbol{\nu}$, which we denote by $\boldsymbol{s}^\nu$, given by

  $$s_k^\nu = s_k^p / s_k^q\,, \quad k = 1, \ldots, N\,.$$

  Next, compute the *IDFT* of the vector $[A^\alpha]^{-1}(\boldsymbol{f} - B^\alpha\boldsymbol{\nu})$, which is the right hand side of (3.4), and which is denoted by $\boldsymbol{s}^\mu$. It is obtained with $O(N)$ operations via

  $$s_k^\mu = \left(s_k^f - s_k^\nu s_k^b\right) / s_k^a\,, \quad k = 1, \ldots, N\,.$$

- **Step 3** Compute the vectors $\boldsymbol{\mu}$ and $\boldsymbol{\nu}$ by taking the *DFT* of the vectors $\boldsymbol{s}^\mu$ and $\boldsymbol{s}^\nu$ respectively.

From the description of the Algorithm it is clear that the total cost of the solution of system (3.1) is $O(N \log N)$ operations.

The implementation of the above algorithm in MATLAB is particularly elegant:

Step 1
```
fa=fft(a); fb=fft(b); fc=fft(c); fd=fft(d);
sf=ifft(f); sg=ifft(g);
```

Step 2
```
sp=sg-sf.*fc./fa;
sn=sp./(fd-fc.*fb./fa);
sm=(sf-sn.*fb)./fa;
```

Step 3
```
m=fft(sm); n=fft(sn);
```

Note that in order to simplify the description of the Algorithm, we have not included some minor modifications which enable us to make additional savings of $O(N)$. For example, the quantities s_k^f/s_k^A need only be computed once in **Step 2**. Further, instead of computing the Schur complement of A^α in G^α after equation (3.2), we could have computed the Schur complement of any of the three matrices B^α, C^α or D^α in G^α. Any of these choices would have yielded an algorithm similar to the one constructed from equations (3.3) and (3.4). Numerical experiments revealed that any of these choices would have had little effect on the behaviour of the error.

4 Numerical Results

We considered the following three examples in Ω with $\varrho = 1$ satisfying problem (1.1). In all three cases the maximum relative error

$$E = \frac{||u - u_N||_\infty}{||u||_\infty}$$

in the approximate solution, is calculated on an $m \times m$ grid defined by the points

$$(r_i \cos\theta_j, r_i \sin\theta_j),\ r_i = \frac{i}{m}, \theta_j = \frac{2\pi(j-1)}{m},\ i, j = 1, \cdots, m.$$

The parameter m is taken to be equal to 101.

4.1 Example 1

We consider the case with $f(x, y) = x^4 - y^4$ and $g(x, y) = 4(x^3 n_x - y^3 n_y)$ which corresponds to the exact solution $u(x, y) = x^4 - y^4$. In Figure 2, we present the maximum error E as $\varepsilon = R - 1$ is varied, for $N = 2^n$, $n = 3, 4, \cdots, 10$. From these results, as expected, the accuracy of the method is poor when $\varepsilon = R - 1$ is either very small or very large. In Figure 3, we present the maximum error E for various $\alpha \in [0, \frac{1}{2})$ for certain values of R. These show that, for small values of ε, the accuracy is sensitive to the value of α. We only consider the interval $[0, \frac{1}{2})$, for the reasons given in section 2.1. In Figure 4, we present a magnification of Figure 3 for certain values of N and R, which reveal an improvement in the accuracy of the method for certain angles α. In Figure 5, we present the maximum error E as the $\varepsilon = R - 1$ is varied, for the values of $N = 2^n$, $n = 3, 4, \cdots, 8$; in the cases when we use the unnormalized fundamental solution approximation (1.3) and when using the normalized fundamental solution approximation with (2.8) and (2.9) as fundamental solutions. This figure reveals that there is a noticeable improvement in accuracy for large values of R when using the normalized fundamental solutions.

4.2 Example 2

In this case we consider a test example from [13], also studied in [16] and [9] where, in polar coordinates, $f(\theta) = -\frac{1}{4}$ and $g(\theta) = -\frac{1}{2}(1 + \cos\theta)$ which corresponds to the exact solution $u(r, \theta) = \frac{1}{4}(1 - r^2)(1 + r\cos\theta) - \frac{1}{4}$. In Figure 6, we present the maximum error E as the radius R is varied, for the values of $N = 2^n$, $n = 3, 4, \cdots, 10$. The behaviour of E is very similar to the corresponding behaviour of E in Example 1, which indicates that the accuracy deteriorates when ε is either very small or very large. In Figure 7, we present the maximum error E as $\alpha \in [0, \frac{1}{2})$ for selected values of N and R. These reveal the sensitivity of the accuracy of the method to the value of α. In Figure 8, we present the maximum error E as the radius R is varied, for the values of $N = 2^4, 2^5, 2^6, 2^7$ for both the standard and the normalized fundamental solutions. As in the previous example, there is an obvious improvement when using the normalized fundamental solutions.

4.3 Example 3

The final and most difficult example describes viscous flow in a circular driven cavity, first studied in [16] and subsequently in [9] and [1], in which

$$f(\theta) = 0$$

and

$$g(\theta) = \begin{cases} -1, & \theta_0 \leq \theta \leq \theta_1 \\ 0, & \theta_1 \leq \theta \leq 2\pi + \theta_0 \end{cases}$$

The exact solution is [16]

$$u(r,\theta) = \frac{(1-r^2)}{2\pi}\left[\gamma + \arctan\left(\frac{1+r}{1-r}\tan\frac{\theta_1-\theta}{2}\right) - \arctan\left(\frac{1+r}{1-r}\tan\frac{\theta_0-\theta}{2}\right)\right],$$

where

$$\gamma = \begin{cases} 0, & \theta_1 - \pi < \theta < \theta_0 + \pi \\ \pi, & \theta_0 + \pi < \theta < \theta_1 + \pi \end{cases}$$

This problem describes the motion of a viscous fluid inside a cylinder, which is generated by the movement of part of its surface at constant speed. The points where the moving surface meets the stationary surface generates two singularities. Thus we have singularities at the points where the boundary condition for the normal derivative changes, that is at the boundary points where $\theta = \theta_0$ and where $\theta = \theta_1$. In Figure 9, we present the maximum error E as the radius R is varied, for the values of $N = 2^n$, $n = 3, 4, \cdots, 10$ in the case $\theta_0 = 0$ and $\theta_1 = \pi$. It can be observed that the error is smallest for a range of values of R, i.e. $R \in (1+\delta_1, 1+\delta_2)$, where $0 < \delta_1 < \delta_2 \ll 1$, close to the boundary because of the boundary singularity. This range becomes narrower and gets closer to the boundary as N increases.

The corresponding results for the case $\theta_0 = \frac{\pi}{4}$ and $\theta_1 = \frac{3\pi}{4}$ are very similar to those of the previous case.

In an effort to improve the accuracy of the method we took a denser grid close to the singular points. Let the total number of collocation points be $N_1 + N_2 = N$, of which N_1+1 correspond to the part of the boundary where where the boundary condition is $g(\theta) = -1$ and $N_2 - 1$ correspond to the part of the boundary where the boundary condition is $g(\theta) = -0$. Then, we took the first $\frac{N_1}{2} + 1$ collocation points to be

$$x_{P_i} = \cos\left(\theta_0 + \frac{(\theta_1 - \theta_0)}{2}\left[\frac{2(i-1)}{N_1}\right]^s\right),$$

$$y_{P_i} = \sin\left(\theta_0 + \frac{(\theta_1 - \theta_0)}{2}\left[\frac{2(i-1)}{N_1}\right]^s\right), \quad i = 1, \ldots, \frac{N_1}{2} + 1,$$

and the next $\frac{N_1}{2}$ collocation points were placed symmetrically about the point $(0,1)$, namely

$$x_{P_{N_1/2+1+i}} = -x_{P_{N_1/2+1-i}}, \;\; y_{P_{N_1/2+1+i}} = y_{P_{N_1/2+1-i}}, \;\; i = 1,\ldots,\frac{N_1}{2}.$$

Similarly, the remaining $N_2 - 1$ collocation points are taken to be

$$x_{P_{N_1+1+i}} = \cos\left(\theta_1 + \frac{2\pi - (\theta_1-\theta_0)}{2}\left[\frac{2i}{N_2}\right]^s\right),$$

$$y_{P_{N_1+1+i}} = \sin\left(\theta_1 + \frac{2\pi - (\theta_1-\theta_0)}{2}\left[\frac{2i}{N_2}\right]^s\right), \;\; i = 1,\ldots,\frac{N_2}{2},$$

$$x_{P_{N_1+1+N_2/2+i}} = -x_{P_{N_1+1+N_2/2-i}}, \;\; y_{P_{N_1+1+N_2/2+i}} = y_{P_{N_1+1+N_2/2-i}}, \;\; i = 1,\ldots,\frac{N_2}{2}-1.$$

The parameter $s \in \mathbb{R}$ determines the density of the collocation points near the singularities. In the case $s = 1$ we have the uniform distribution of equation (1.6), while for $s > 1$ we have a denser distribution of collocation points near the singularities, the density increasing with s. In a similar way, singularities were placed at

$$x_{Q_i} = R\, x_{P_i}, \;\; y_{Q_i} = R\, y_{P_i}, \;\; i = 1,\ldots,N.$$

In Figure 10, we present the concentration of the boundary points for various degrees of density, namely $s = 1$, $s = 1.2$ and $s = 1.4$ when $N = 128$, in the case $\theta_0 = 0$ and $\theta_1 = \pi$. In the same figure we also present the corresponding graphs of the maximum error E versus the radius R. From Figure 10 we can see the improvement in accuracy as the density factor s increases. However, the range of values of R for which this improvement occurs decreases as s and N increase.

In Figure 11, we present the graph of E versus R, for the values of $N = 2^7, 2^8, 2^9, 2^{10}$ in the case $\theta_0 = \frac{\pi}{4}$ and $\theta_1 = \frac{3\pi}{4}$ and the values of $s = 1, 1.3, 1.6, 1.9, 2.2$. Again, an improvement in the accuracy is observed as s increases. As in the previous case, however, the range of values of R for which this improvement occurs decreases as s and N increase.

Note that the range of values of s for which there is an improvement in the accuracy of the method is quite different in the two cases examined. In the case when the singularities are closer to each other, a denser concentration of boundary points is needed to produce more accurate results.

In Figures 12 and 13 we present the contour plots of the streamfunction in the cases $\theta_0 = 0$ and $\theta_1 = \pi$, and $\theta_0 = \frac{\pi}{4}$ and $\theta_1 = \frac{3\pi}{4}$, respectively, obtained with $N = 2^{10}$. These are in excellent agreement with the corresponding plots in the literature (see e.g. [1]). Finally, in Figure 14 we present the contour plot of the vorticity in the case $\theta_0 = 0$ and $\theta_1 = \pi$.

The idea of using a denser boundary grid close to boundary singularities has also been used with the MFS in [8]. It should be noted that for values of $s \neq 1$ the matrices A^0, B^0, C^0 and D^0 are no longer circulant. In this example, experiments with rotated singularities ($\alpha > 0$) failed to produce any improvement in the accuracy of the results.

5 Summary

We examined some of the shortcomings associated with the numerical solution of the homogeneous biharmonic equation in circular geometries with the MFS. In particular, we examined ways of overcoming the poor accuracy of the method when the singularities are placed either very close to or very far from the boundary. In the case where the circle on which the singularities are placed is located very close to the boundary, numerical experiments revealed that the angular positioning of these is of crucial importance. In the case where this artificial boundary is located very far from the boundary, a normalization of the fundamental solutions leads to improved accuracy. Exploiting the fact that the matrices involved in the above approaches can be written as a block of circulant matrices, leads to an efficient algorithm for the solution of the resulting systems. It should be noted that this algorithm is only applicable in the case of the specific problem examined.

We also examined a problem with boundary singularities where it was observed that the accuracy of the method was poor except when the singularities were placed on a circle very close to the boundary. This is expected, as the method is only applicable to problems the solution of which is analytically continuous across the boundary. In this case, a denser concentration of boundary collocation points (and singularities) close to the boundary singularities produced improved results.

Preliminary numerical experiments were also carried out in the case when Ω is not a disk. It should be noted that when Ω is not a disk, the corresponding matrix G cannot be decomposed into four circulant matrices and the efficient algorithm developed in section 3.3 cannot be applied. In particular, we carried out numerical tests when Ω is a rectangle and the exact solution is that of Example 1. These revealed that the same phenomena persist, namely the numerical results are poor when the singularities are placed either very close or very far from the boundary. We also performed numerical experiments in the case of the driven cavity problem in a square region. As in the case of the circular driven cavity, a denser concentration of boundary collocation points (and singularities) near the boundary singularities, improves the accuracy of the method.

Acknowledgement

The authors wish to thank Professor Graeme Fairweather of the Colorado School of Mines for his useful comments. We are also grateful to the two anonymous referees for their constructive commnents.

References

[1] Z. Belhachmi, C. Bernardi and A. Karageorghis, *Spectral element discretization of the circular driven cavity. Part II: The bilaplacian equation*, SIAM J. Numer. Anal., 38, 1926 - 1960, 2001.

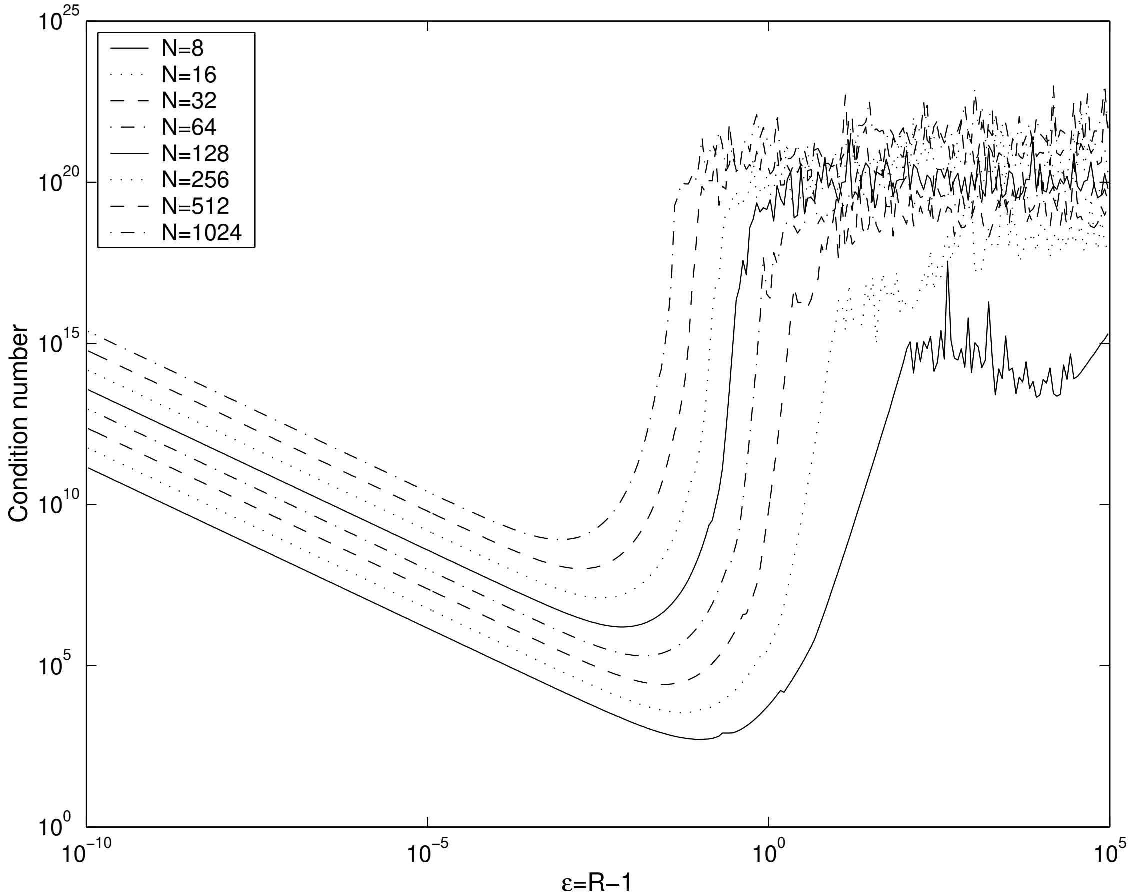

Figure 1: Condition number versus $\varepsilon = R - 1$.

[2] A. Bogomolny, *Fundamental solutions method for elliptic boundary value problems*, SIAM J. Numer. Anal., 22, 644-669, 1985.

[3] P. J. Davis, *Circulant Matrices*, John Wiley and Sons, New York, 1979.

[4] A. Doicu, Yu. Eremin and T. Wriedt, *Acoustic and Electromagnetic Scattering Analysis Using Discrete Sources*, Academic Press, New York, 2000.

[5] G. Fairweather and A. Karageorghis, *The method of fundamental solutions for elliptic boundary value problems*, Adv. Comput. Math., 9, 69-95, 1998.

[6] M. A. Golberg and C. S. Chen, *Discrete Projection Methods for Integral Equations*, Computational Mechanics Publications, Southampton, 1996.

[7] M. A. Golberg and C. S. Chen, *The method of fundamental solutions for potential, Helmholtz and diffusion problems*, in: *Boundary Integral Methods and Mathematical Aspects*, ed. M. A. Golberg, WIT Press/Computational Mechanics Publications, Boston, 1999, pp. 103-176.

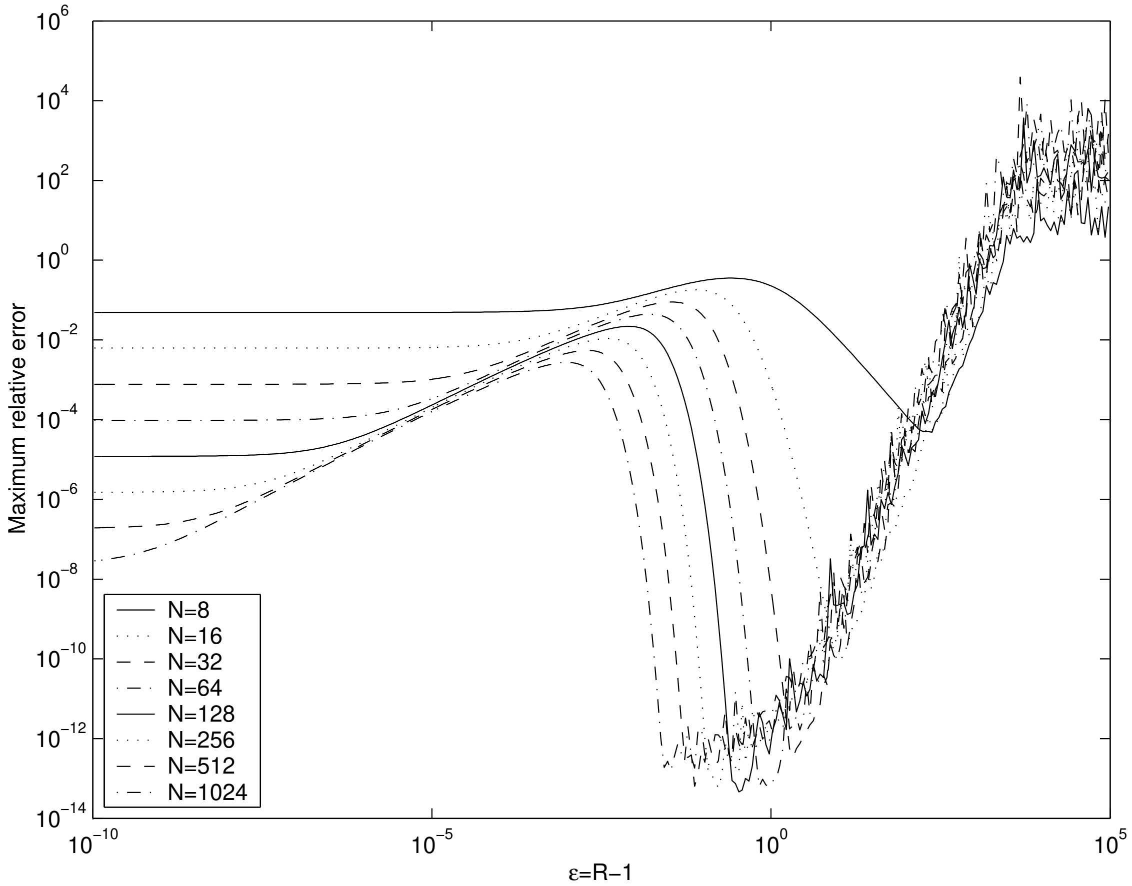

Figure 2: Maximum relative error versus $\varepsilon = R - 1$ in Example 1.

[8] A. Karageorghis and G. Fairweather, *The method of fundamental solutions for the numerical solution of the biharmonic equation*, J. Comp. Phys., 69, 434-459, 1987.

[9] A. Karageorghis and T. Tang, *A spectral domain decomposition approach for steady Navier-Stokes problems in circular geometries*, Computers & Fluids, 25, 541-549, 1996.

[10] J. A. Kolodziej, *Applications of the Boundary Collocation Method in Applied Mechanics*, Wydawnictwo Politechniki Poznanskiej, Poznan, 2001. (In Polish).

[11] V. D. Kupradze, *Potential Methods in the Theory of Elasticity*, Israel Program for Scientific Translations, Jerusalem, 1965.

[12] V. D. Kupradze and M. A. Aleksidze, *The method of functional equations for the approximate solution of certain boundary value problems*, U.S.S.R. Comp. Math. and Math. Phys. 4, 82-126, 1964.

[13] K. Kuwahara and I. Imai, *Steady, viscous flow with circular boundary*, Phys. Fluids Supple., 12, II-94 -II-101, 1969.

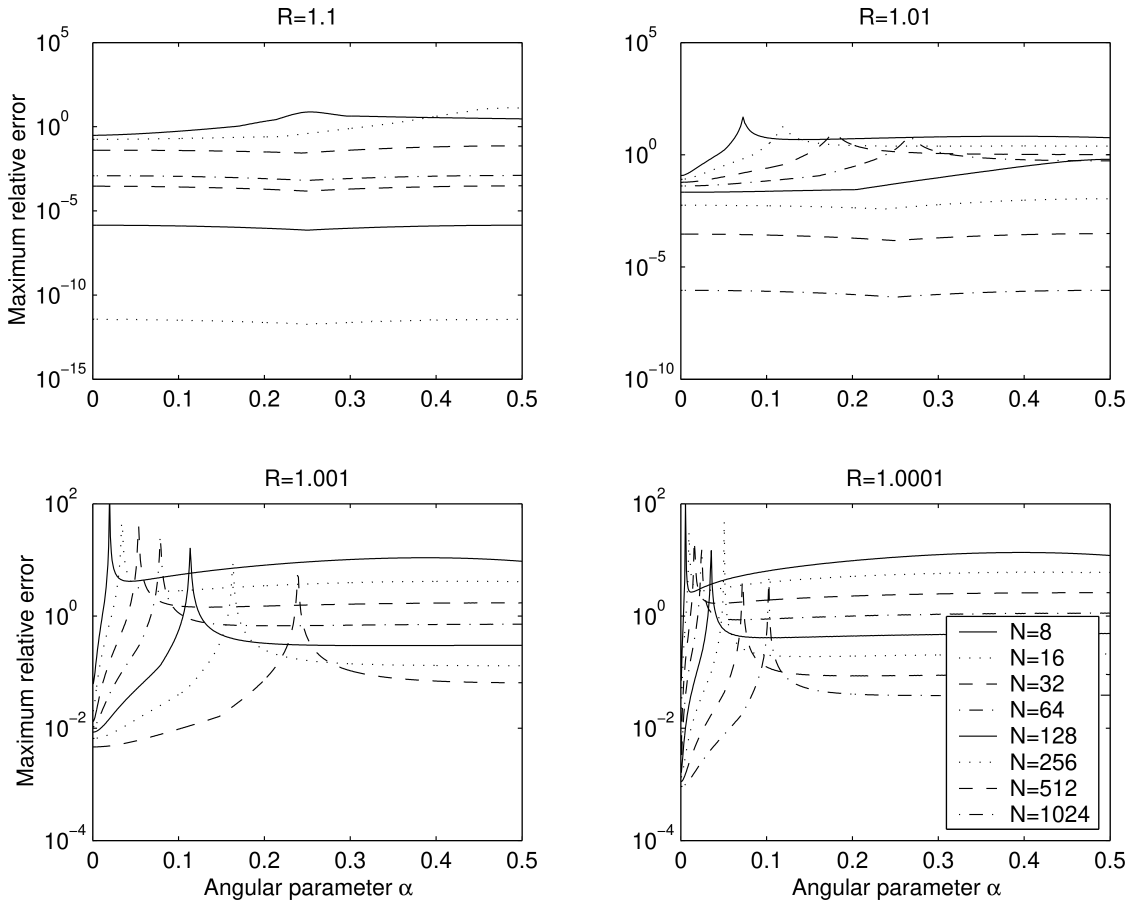

Figure 3: Maximum relative error versus angular parameter in Example 1.

[14] M. Maiti and S. K. Chakrabarti, *Integral equation solutions for simply supported polygonal plates*, Int. J. Engng. Sci., 12, 793-806, 1974.

[15] R. Mathon and R. L. Johnston, *The approximate solution of elliptic boundary-value problems by fundamental solutions*, SIAM J. Numer. Anal., 14, 638-650, 1977.

[16] R. D. Mills, *Computing internal viscous flow problems for the circle by integral methods*, J. Fluid Mech., 79, 609-624, 1977.

[17] *Numerical Algorithms Group Library Mark 19*, NAG Ltd, Wilkinson House, Jordan Hill Road, Oxford, UK, 1999.

[18] Y.S. Smyrlis and A. Karageorghis, *Some aspects of the method of fundamental solutions for certain harmonic problems*, J. Sci. Comp., 16, 341-371, 2001.

[19] G. W. Stewart, *Matrix Algorithms, Volume I: Basic Decompositions*, SIAM, Philadelphia, 1998.

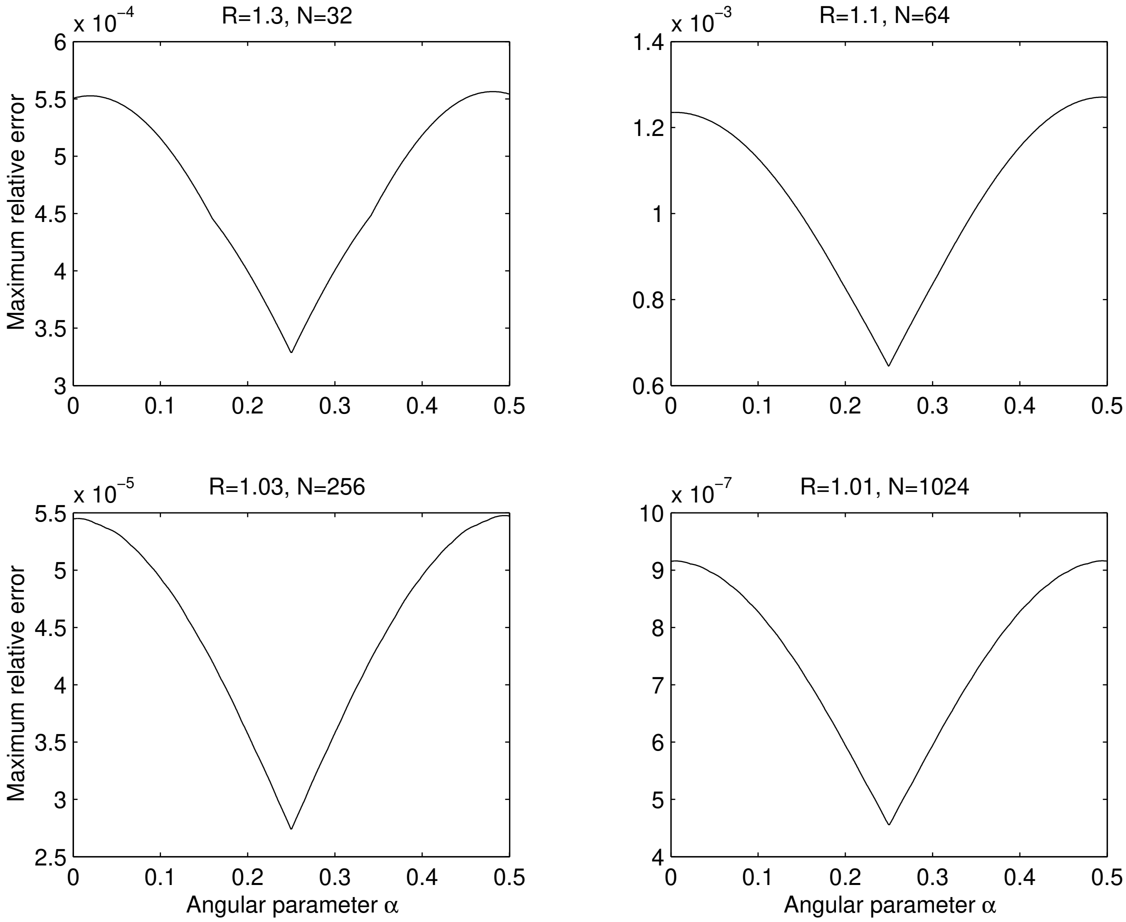

Figure 4: Magnified plots of error versus angular parameter in Example 1.

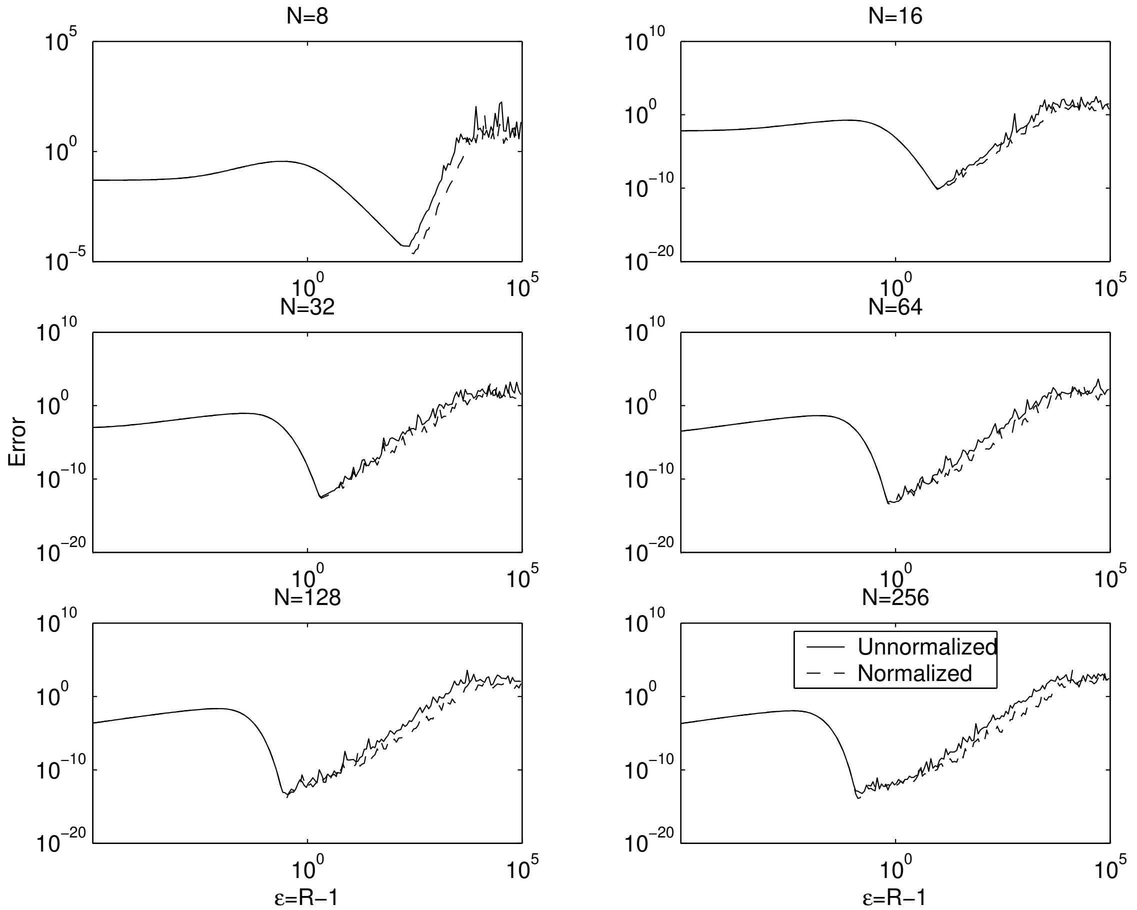

Figure 5: Approximation with normalized versus unnormalized fundamental solutions in Example 1.

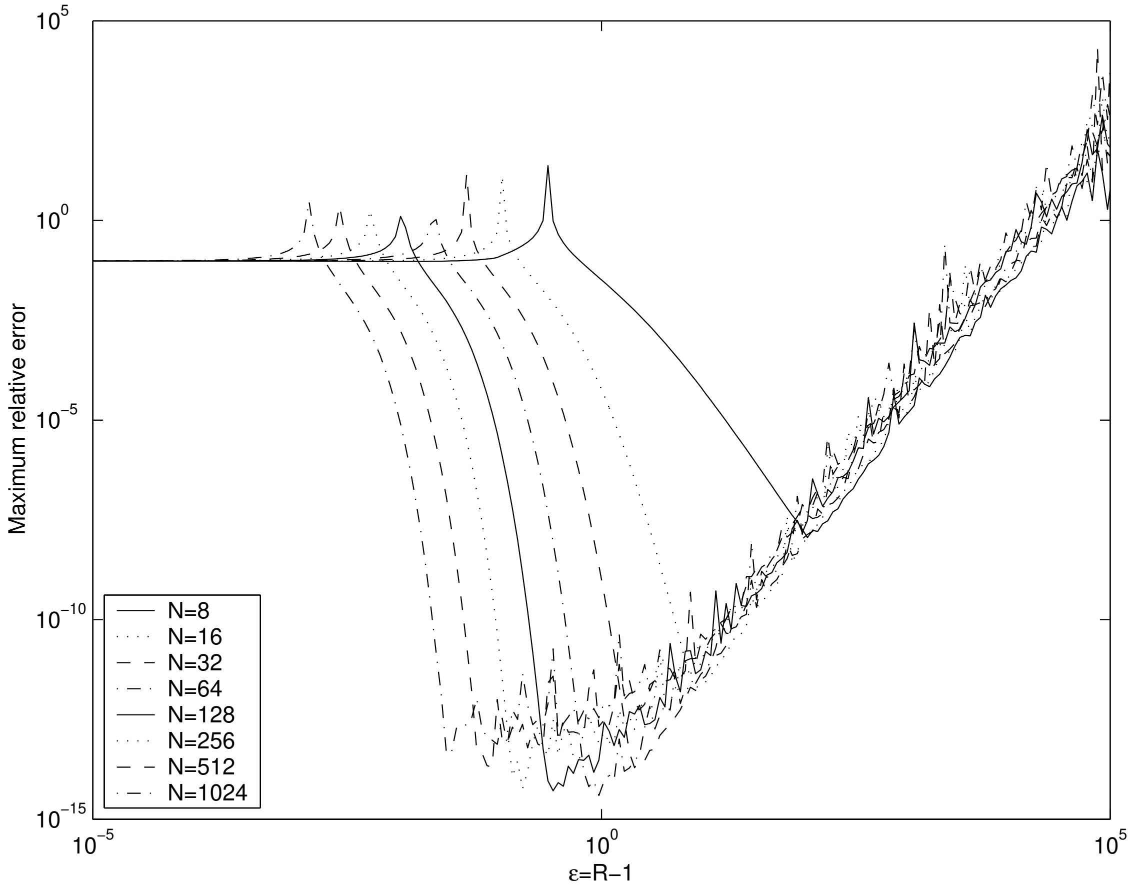

Figure 6: Maximum relative error versus $\varepsilon = R - 1$ in Example 2.

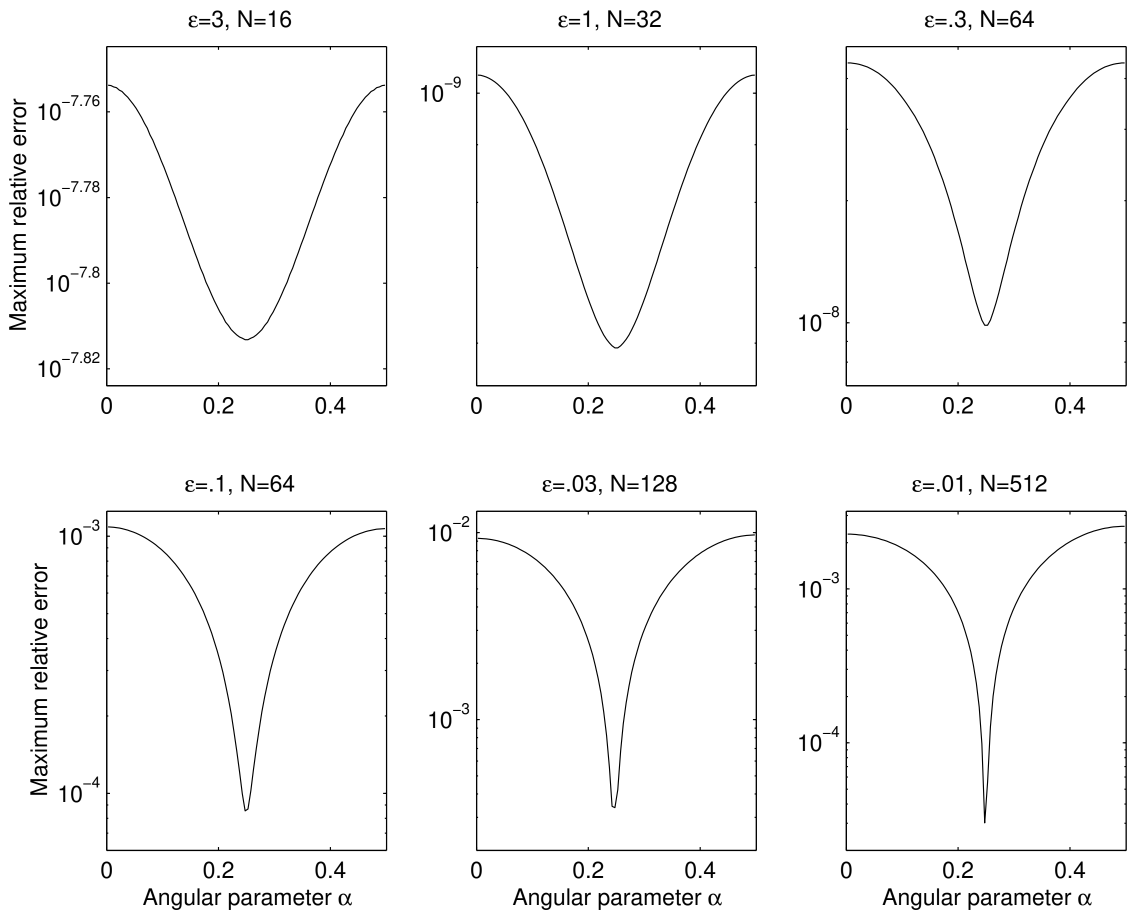

Figure 7: Selected plots of error versus angular parameter in Example 2.

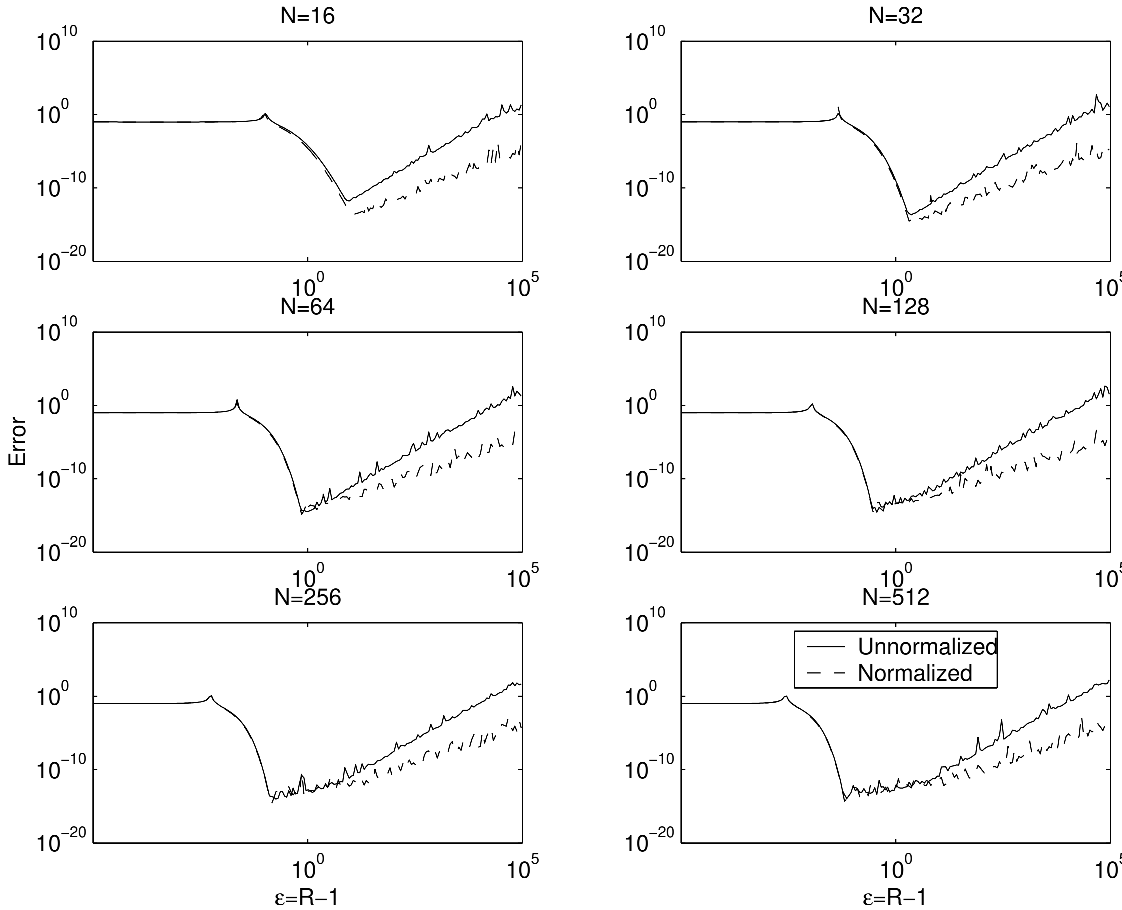

Figure 8: Approximation with normalized versus unnormalized fundamental solutions in Example 2.

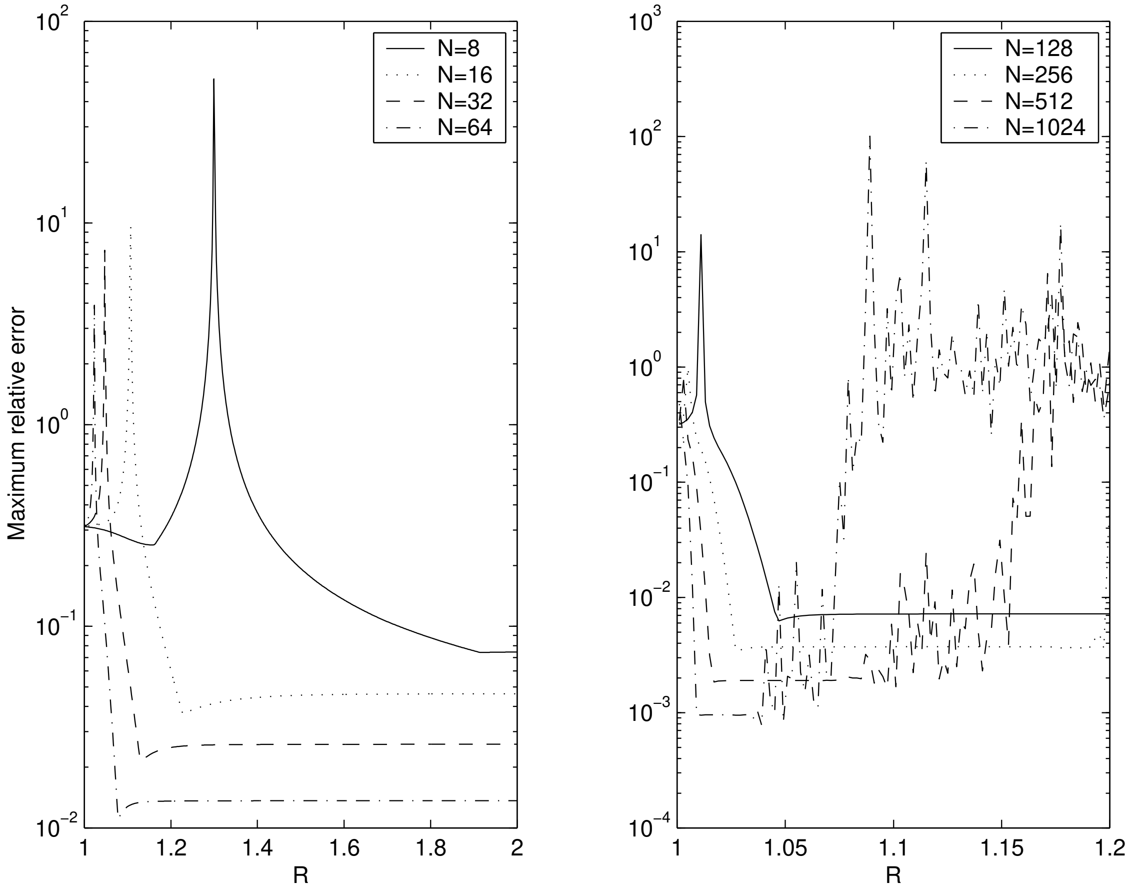

Figure 9: Maximum relative error versus the radius R in Example 3 in the case $\theta_0 = 0$ and $\theta_1 = \pi$.

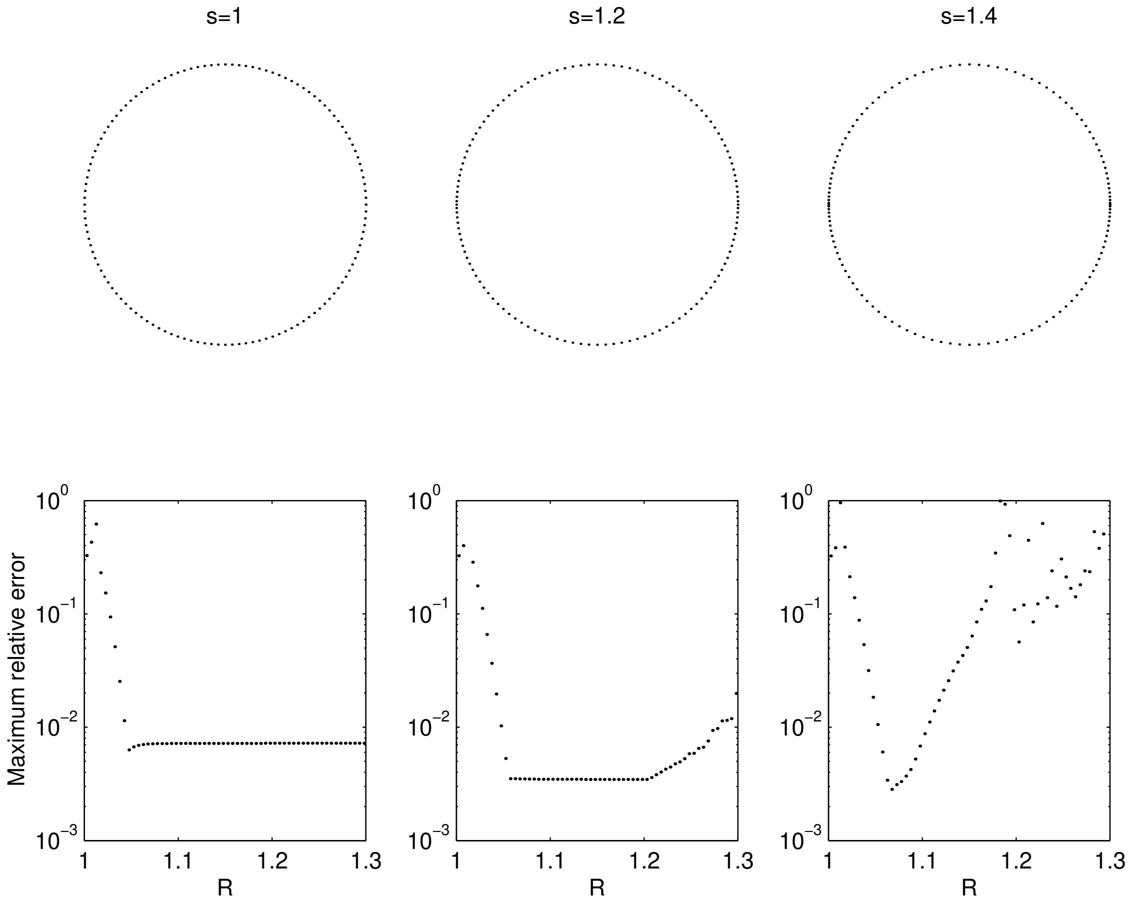

Figure 10: Concentration of boundary points for the values $s = 1$, $s = 1.2$ and $s = 1.4$ with corresponding maximum relative error versus R graphs for $N = 128$ in Example 3, in the case $\theta_0 = 0$ and $\theta_1 = \pi$.

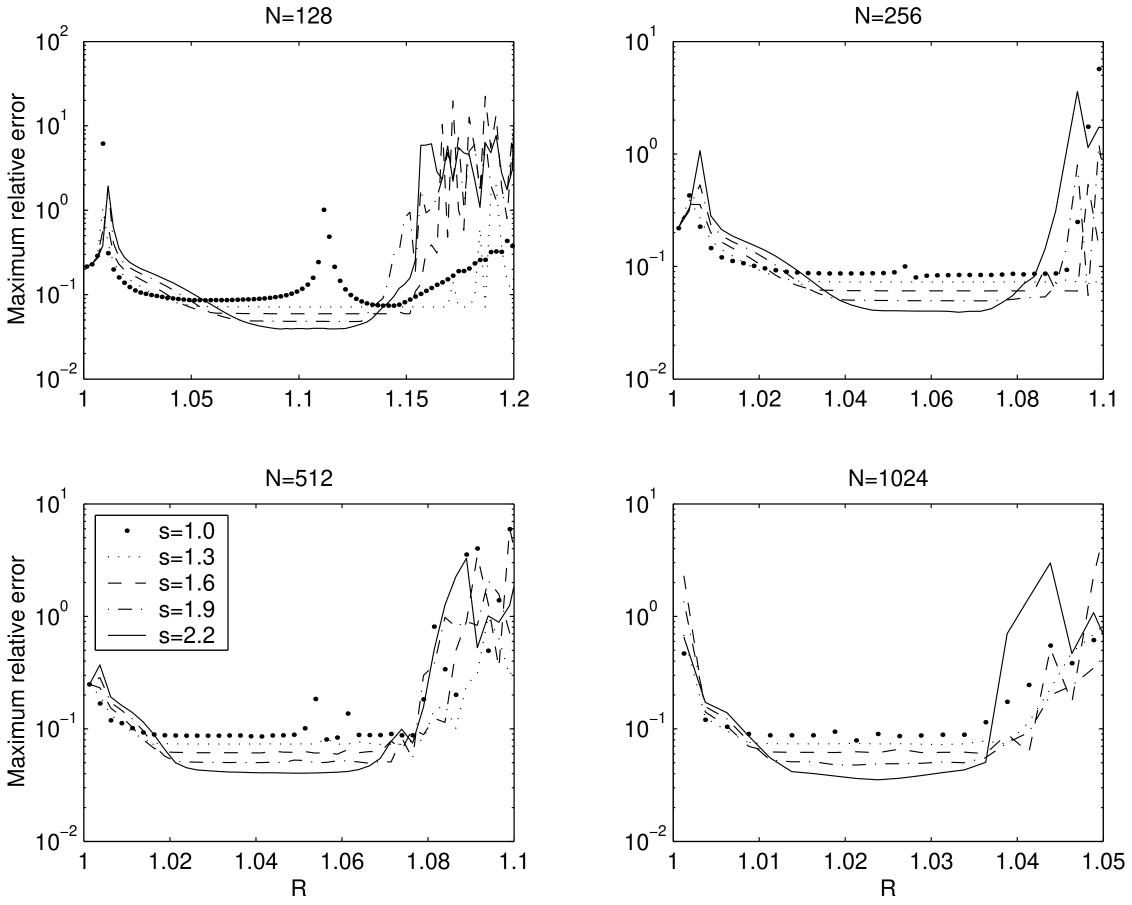

Figure 11: Maximum relative error versus the radius R in Example 3 for various degrees of density of the collocation points and the singularities in the case $\theta_0 = \frac{\pi}{4}$ and $\theta_1 = \frac{3\pi}{4}$.

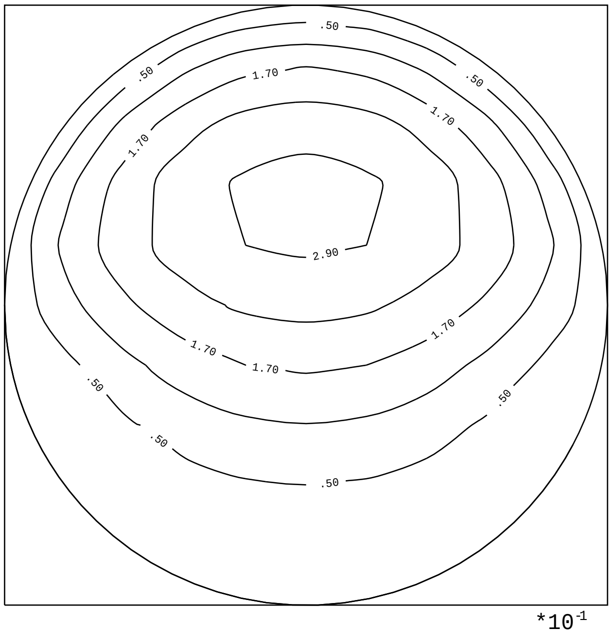

Figure 12: Contour plot of the streamfunction for Example 3 in the case $\theta_0 = 0$ and $\theta_1 = \pi$.

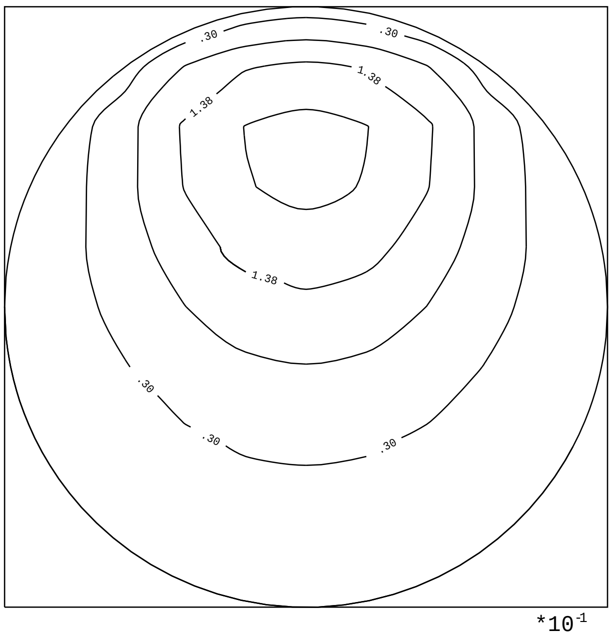

Figure 13: Contour plot of the streamfunction for Example 3 in the case $\theta_0 = \frac{\pi}{4}$ and $\theta_1 = \frac{3\pi}{4}$.

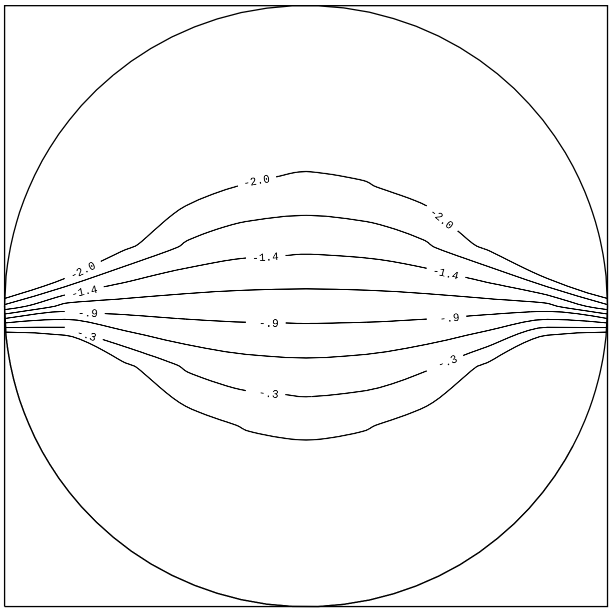

Figure 14: Contour plot of the vorticity for Example 3 in the case $\theta_0 = 0$ and $\theta_1 = \pi$.